

Effect of non-metallic silicon content on the microstructure and corrosion behaviour of AlCoCrFeNi high-entropy alloys

Yi Wang ^{a,b}, Guanglong Li ^{a,b,*}, Hao Qi ^{a,b}, Wei Zhang ^{a,b}, Ruirun Chen ^c, Ruiming Su ^{a,b}, Bo Yu ^d, Yingdong Qu ^{a,b,**}

^a School of Materials Science and Engineering, Shenyang University of Technology, Shenyang, 110870, China

^b Key Laboratory of Light Metal Materials and Engineering at Universities of Liaoning Province, Shenyang, 110870, China

^c National Key Laboratory for Precision Hot Processing of Metals, Harbin Institute of Technology, 150001, China

^d China Academy of Machinery Shenyang Research Institute of Foundry Co., Ltd., Shenyang, 110022, China

HIGHLIGHTS

- AlCoCrFeNi high-entropy alloys (HEAs) with varied Si contents prepared.
- Corrosion resistance of the HEAs in 3.5 wt% NaCl solution investigated.
- AlCoCrFeNiSi_{0.2} HEAs has the optimal corrosion resistance.
- Corrosion mechanism of AlCoCrFeNiSi_x HEAs elucidated.

ARTICLE INFO

Keywords:
AlCoCrFeNiSi_x
Spinodal decomposition
Passivation film
General corrosion
Localised corrosion

ABSTRACT

AlCoCrFeNi high-entropy alloys (HEAs) have shown excellent mechanical properties and high-temperature oxidation resistance but poor corrosion resistance owing to the high contents of the aluminium passivation film. In this study, Si was added to these alloys with the aim of improving the composition and stability of the passivation films. The microstructure and corrosion behaviour of AlCoCrFeNiSi_x (molar ratio x = 0, 0.1, 0.2, 0.3, and 0.4) HEAs were investigated. Dendritic and spinodal decomposition regions were observed in all five alloys. In the dendritic region, the dendritic structures transitioned from a petal shape to a dendritic shape with increasing Si content. Phase separation occurred in the spinodal decomposition region, which predominantly consisted of ordered body-centred cubic (B2) and disordered body-centred cubic (A2) phases. The size of the A2 phase decreased, and the amount of the A2 phase increased with increasing Si content. An optimised Si content could enhance the stability of Al and Cr passivation films, whereas excessive Si imposed an adverse effect by forming a Cr passivation film. The corrosion resistance of AlCoCrFeNiSi_{0.2} HEAs was optimum with a passive current density of 3.2 $\mu\text{A}/\text{cm}^2$, which was 0.2 times that of the obtained AlCoCrFeNi HEAs without Si. The type of corrosion changed from local corrosion of AlCoCrFeNiSi_x ($x \leq 0.3$) HEAs to general corrosion of AlCoCrFeNiSi_{0.4} HEAs. The corrosion mechanisms of the AlCoCrFeNi HEAs with various Si contents were elucidated.

1. Introduction

Al_xCoCrFeNi high-entropy alloys (HEAs) were first reported in 2008 [1] and are currently one of the most developed and complete HEA systems [2,3]. Al is regarded as a stabiliser of body-centred cubic (BCC) structures owing to its large atomic size [4,5], which can improve the strength [6–8] and oxidation resistance [9–11] of Al_xCoCrFeNi HEAs.

Therefore, Al plays an indispensable role in Al_xCoCrFeNi HEAs. However, recent studies have shown that the corrosion resistance of Al_xCoCrFeNi HEAs gradually decreases with the addition of Al [12,13]. Most studies have focused on finding other elements to substitute for Al [14,15]; however, the performance (e.g., hardness, strength, and oxidising resistance) of AlCoCrFeNi HEAs decreases with the disappearance of Al. Therefore, improving the corrosion resistance of AlCoCrFeNi HEAs

* Corresponding author. School of Materials Science and Engineering, Shenyang University of Technology, Shenyang, 110870, China.

** Corresponding author. School of Materials Science and Engineering, Shenyang University of Technology, Shenyang, 110870, China.

E-mail addresses: liguanglong1990@163.com (G. Li), quydong@sut.edu.cn (Y. Qu).

without reducing their Al content has become an important research topic.

The performance of traditional alloys can be enhanced by adding appropriate amount of non-metallic Si. However, extant corrosion studies of such HEAs are prominently focused on changes in metallic elements, and few studies have focused on the addition of non-metallic elements such as Si. Xiang et al. [16] investigated the corrosion resistance of AlCoCrFeNiSi_{0.1} HEAs and compared it with that of stainless steel 304 (SS304). The results showed that the corrosion behaviour of the AlCoCrFeNiSi_{0.1} HEAs was slightly better than that of SS304. Chen et al. [17] analysed the corrosion resistance of FeCoNiAl_{0.2}Si_{0.2} HEAs via rapid solidification and slow cooling. They found that a passivation film of SiO₂ was generated by rapid solidification, thereby improving the corrosion behaviour of HEAs. Li et al. [18] studied the effect of Si on the oxidation resistance of AlCoCrFeNi alloy at 1100 °C for 200 h. The results show that the addition of a suitable amount of Si can form a compact oxide film of Al₂O₃. Gorr et al. [19] studied the oxidation behaviour of Nb–Mo–Cr–Ti–Al HEAs with and without Si element at 900, 1000, and 1100 °C. They found that the surface of Nb–Mo–Cr–Ti–Al HEAs formed a near-continuous Al-rich oxide film upon adding Si; this could enhance the oxidation behaviour. According to above, Si can improve the driving force of Al oxide films during oxidation. Although the formation environments of Al oxide and Al passivation films are different, their compositions are theoretically related. It is inferred that an increasing non-metallic Si content may have a positive impact on the Al passivation film of AlCoCrFeNi HEAs.

Zhu et al. [20] prepared AlCoCrFeNi HEAs with various Si contents (molar ratios of 0, 0.2, 0.4, 0.6, 0.8, and 1.0) and found that AlCoCrFeNiSi_{0.4} HEAs exhibits excellent comprehensive mechanical properties, yield stress of 1481 MPa, fracture strength of 2444 MPa and plastic strain of 13.38 %, respectively. The improvement of mechanical properties is attributed to the solid solution of Si element and precipitation strengthening of nanoscale cellular structure. However, no study has focused on the corrosion behaviour of AlCoCrFeNiSi_x HEAs thus far. Mechanical stress and corrosion are perfect combinations for the evaluation of alloys. Investigating corrosion resistance is essential for the development of new alloys. Therefore, studying the corrosion resistance of AlCoCrFeNi alloys with various Si contents is imperative.

AlCoCrFeNi HEAs with various Si contents (molar ratios of 0, 0.1, 0.2, 0.3, and 0.4) were designed and prepared in this study. The corrosion resistances of the AlCoCrFeNiSi_x HEAs were analysed in 3.5 wt % NaCl solution from two aspects: passivation film and crystal structure. The purpose of the present study was twofold: (a) to improve the corrosion resistance of AlCoCrFeNi HEAs and (b) to investigate the corrosion mechanism of AlCoCrFeNiSi_x HEAs.

2. Materials and methods

2.1. Material and sample preparation

The AlCoCrFeNiSi_x ($x = 0.0, 0.1, 0.2, 0.3, 0.4$) HEAs were prepared via vacuum arc melting, as shown in Table 1. The raw materials consisted of six elements: Al, Co, Cr, Fe, Ni, and Si with 99.99 % purity or higher. Approximately 70 g of ingots was re-melted at least five times in a water-cooled Cu crucible under a high-purity argon atmosphere to

ensure chemical homogeneity (the furnace environment reached a vacuum state of 5×10^{-3} Pa). The samples were smelted five times to ensure homogeneity.

2.2. Corrosion test

Using wire cutting, the test sample was cut into a size of 10 mm × 10 mm × 10 mm, and the surface of the sample was ground using sandpaper to 2000#. Potential polarisation, impedance, and Mott–Schottky experiments were performed using an electrochemical workstation system (DH7000, Jiangsu Donghua Analytical Instruments Co., Ltd.) in 3.5 wt % NaCl solution. A platinum plate was used as the auxiliary electrode, a saturated calomel electrode (SCE) was used as the reference electrode, and the sample was used as the working electrode to form a three-electrode system. All electrochemical measurements were conducted at room temperature (25 °C). First, the working electrode cathodic polarisation was performed at -800 mV_{SCE} for 5 min to reduce the possible surface oxides. The steady-state polarisation measurement was conducted at scan rates from 10 to 1000 mV/min; the initial potential is taken at -0.4 V_{SCE}. The sinusoidal potential amplitude of the impedance was 10 mV, starting from 100 kHz to 10 mHz. The equivalent circuit of the impedance data was fitted using the ZsimpWin software (version 3.0). Mott–Schottky measurements were performed from -1000 to 1000 mV_{SCE} with a step size of 10 mV at a frequency of 1 kHz. To ensure data accuracy, all electrochemical measurements were performed at least three times.

2.3. Chemical and microstructural characterisation

The size of the test sample was 10 mm × 10 mm × 10 mm, which was achieved by wire cutting, and the surface of the sample was ground using sandpaper to 2000 #. To improve the surface roughness of the samples, an electrolytic polishing method was used to polish the surface (voltage: 27 V and current: 1 A). The phase composition of the AlCoCrFeNiSi_x HEAs was analysed via X-ray diffraction (XRD; XRD-7000, Shimadzu, Kyoto, Japan) over a scattering angle (2θ) range of 20°–90° at a scan rate of 2°/min. The microstructure was studied using scanning electron microscopy (SEM; GeminiSEM 300, ZEISS) before and after corrosion, and the elemental distribution was analysed using energy-dispersive spectroscopy (EDS). In addition, the morphology of the corroded sample surface was analysed using laser confocal microscopy (LEXT OLS4100, Olympus). The microstructures were observed via transmission electron microscopy (TEM; JEM-2100, JEOL) operated at 200 kV. The oxide film on the surface of the AlCoCrFeNiSi_x HEAs was analysed using X-ray photoelectron spectrometry (XPS; ESCALAB 250Xi, Thermo Fisher Scientific), and the high-resolution spectra were fitted using Advantage software.

3. Results

3.1. Microstructural characterisation

Fig. 1 shows the XRD patterns of the AlCoCrFeNiSi_x HEAs; AlCoCrFeNiSi_{0.0} are denoted as Si-0.0 HEAs, and the others are also modified. The AlCoCrFeNiSi_x HEAs are displayed as a solid-solution phase of disordered BCC (A2). When Si molar ratio ≥ 0.1 , superlattice reflection (100)_{B2} phase, which has a correlation with ordered BCC phase, begins to appear. This indicates that the phase structure does not change with the addition of Si but promotes phase separation. In addition, when Si molar ratio ≥ 0.2 , some silicide could be detected clearly, such as Ni₃₁Si₁₂, Ni₃Si, Ni₃Si, CrFe₅Si, Cr₃Si, CrSi₂ and all the rest of it [21], in this work the silicide was identified as being CrSi₂ via XRD. **Fig. 1** shows a local enlarged main peak, which shifts slightly to the right with an increasing Si content. This indicated that the addition of Si decreased the lattice parameter and reduced the interplanar spacing.

Fig. 2 shows the structural morphology of AlCoCrFeNi HEAs with

Table 1
Nominal compositions of AlCoCrFeNiSi_x HEAs.

Alloys	Element (at.%)					
	Al	Co	Cr	Fe	Ni	Si
AlCoCrFeNiSi _{0.0}	20.00	20.00	20.00	20.00	20.00	0.00
AlCoCrFeNiSi _{0.1}	19.61	19.61	19.61	19.61	19.61	1.95
AlCoCrFeNiSi _{0.2}	19.23	19.23	19.23	19.23	19.23	3.85
AlCoCrFeNiSi _{0.3}	18.87	18.87	18.87	18.87	18.87	5.65
AlCoCrFeNiSi _{0.4}	18.52	18.52	18.52	18.52	18.52	7.40

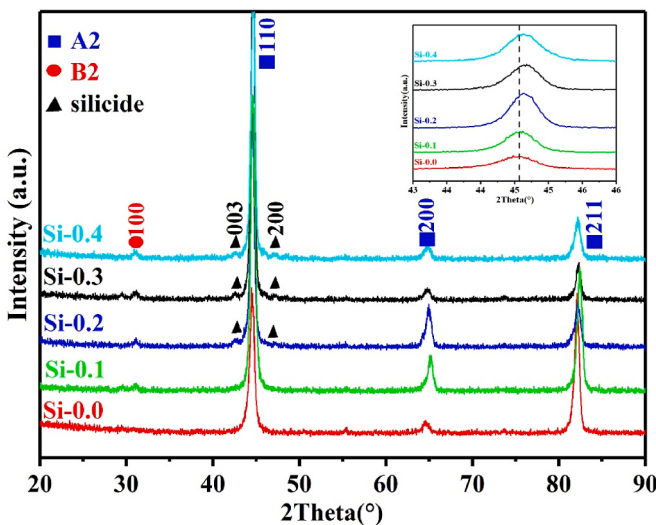


Fig. 1. XRD pattern of AlCoCrFeNiSi_x ($x = 0, 0.1, 0.2, 0.3$, and 0.4) HEAs.

various Si contents. The dark and light regions represent the dendritic region (DR) and the spinodal decomposition region (disordered BCC A2 phase and ordered BCC B2 phase), respectively. The crystal structure of the Si-0.1 HEAs was similar to that of the Si-0.0 HEAs and was composed primarily of a DR (petal-like) and a spinodal decomposition region. When Si molar ratio ≥ 0.2 , spinodal decomposition was still observed, and the DR transformed from a petal-like structure to a dendritic-like

structure. The results indicated that the addition of Si promoted composition segregation, which changed the morphology of the DRs.

The distribution of Si in Si-0.4 HEAs was analysed using EDS (Fig. 3). The DR is rich in the Al-Ni phase, the inter-dendritic region (ID) is enriched with the Fe-Cr-Si phase, and Co is uniformly distributed in the Si-0.4 HEAs. The enthalpies of mixing of Si with Al, Co, Cr, Fe, and Ni are -19 , -38 , -19 , -35 , and -40 kJ/mol, respectively [22], indicating that Si has a strong binding force with other elements of AlCoCrFeNi HEAs. According to the EDS results shown in Fig. 3, it is reasonable to speculate that Si combines with Fe and Cr to segregate in the ID region.

3.2. Electrochemical determination

3.2.1. Electrochemical polarisation test

The corrosion potential (E_{corr}), corrosion current density (i_{corr}), passive current density (i_{pass}), and pitting potential (E_{pit}) of the AlCoCrFeNiSi_x HEAs were characterised using the Tafel fitting method, as shown in Fig. 4 and Table 2. Generally, the corrosion current density belongs to the kinetics mechanism, which is the chief gauge of corrosion behaviour [23,24] lower the value of i_{corr} , the better would be the corrosion resistance. However, AlCoCrFeNiSi_x HEAs have clear passivation areas, and the Tafel extrapolation method is not strictly valid for determining i_{corr} [25,26]. Therefore, we should rely on the i_{pass} value as a measure of the anodic dissolution rate rather than on the i_{corr} values. Thus, according to the i_{pass} value, the corrosion resistance densities from the highest to the lowest were the Si-0.2, Si-0.1, Si-0.0, Si-0.3, and Si-0.4 HEAs. The corrosion resistances of AlCoCrFeNiSi_x HEAs show a trend from ascent to descent.

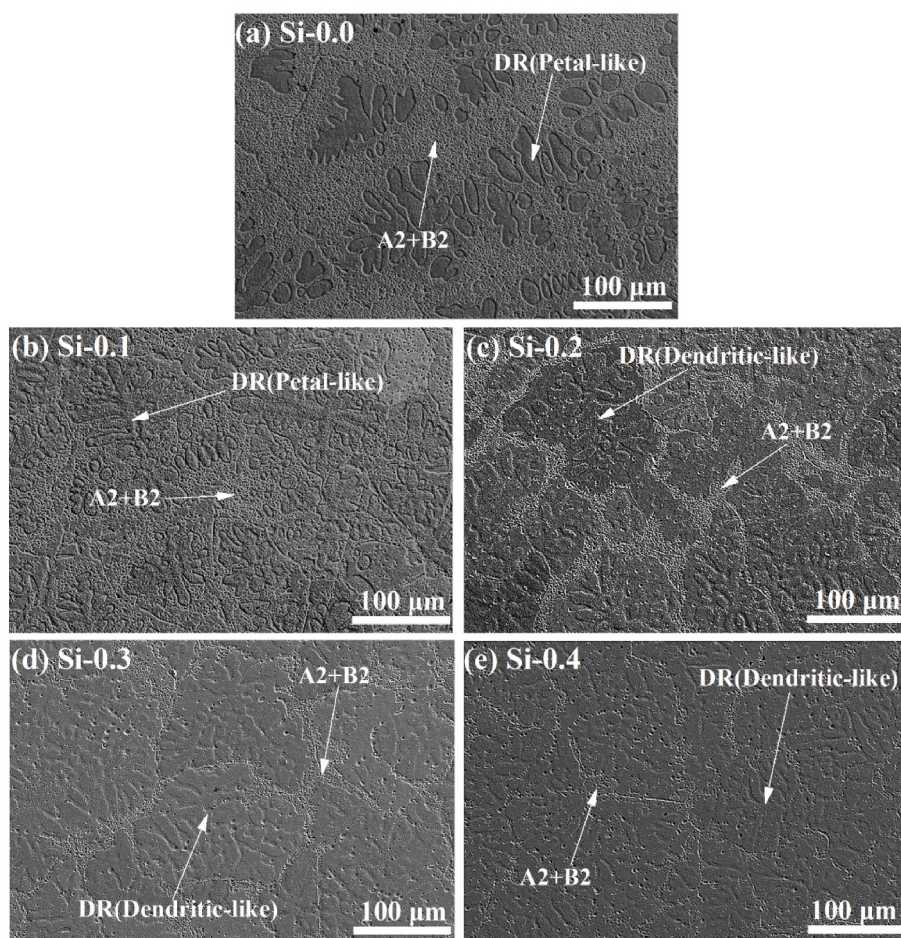


Fig. 2. SEM micrographs of AlCoCrFeNiSi_x ($x = 0.0, 0.1, 0.2, 0.3$, and 0.4) HEAs.

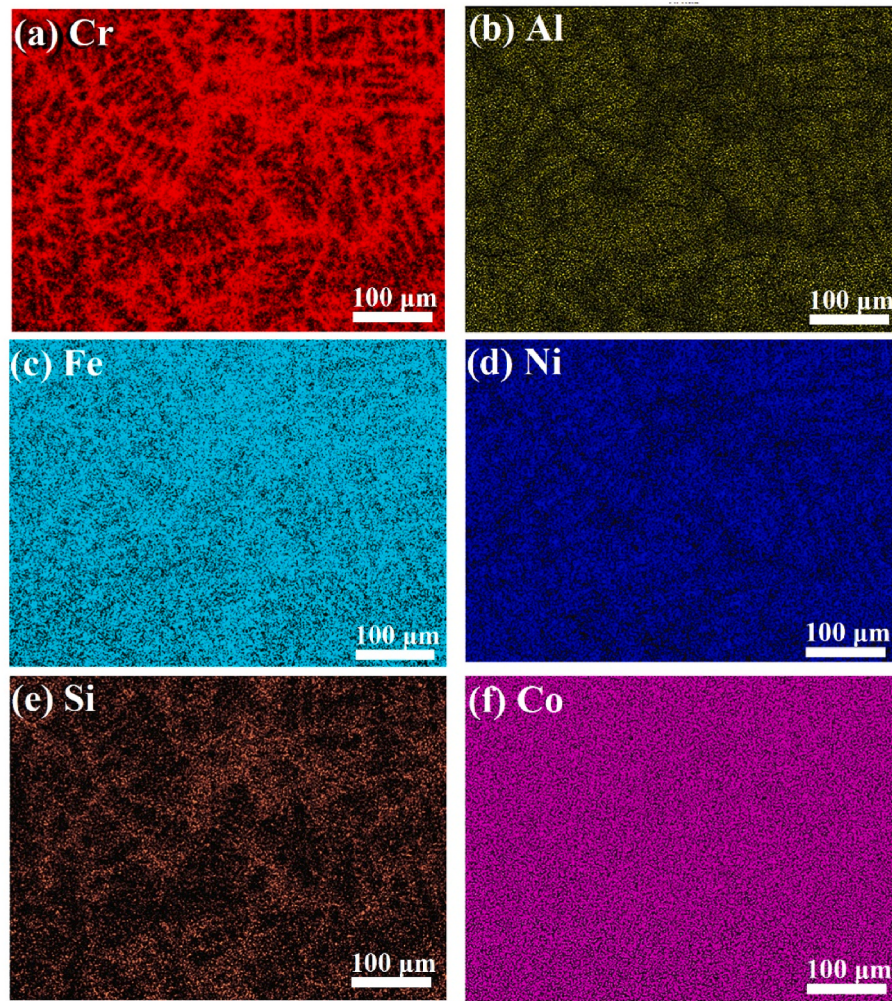


Fig. 3. EDS of AlCoCrFeNiSi_{0.4} HEAs.

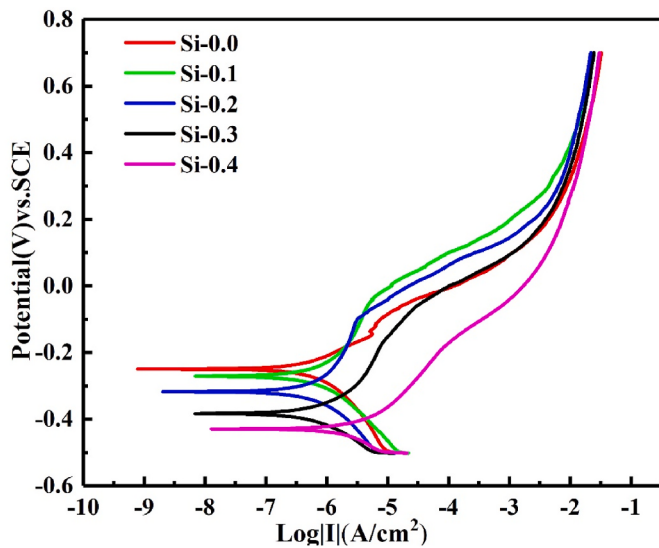


Fig. 4. Electrochemical polarisation curve of AlCoCrFeNiSi_x HEAs.

3.2.2. EIS measurements

Fig. 5 shows the electrochemical impedance spectroscopy (EIS) results for the AlCoCrFeNiSi_x HEAs. An unfinished semi-arc is present in

Table 2

Specific values of the electrochemical parameter in AlCoCrFeNiSi_x HEAs.

Alloys	E_{corr} (mV _{SCE})	i_{corr} ($\mu\text{A}/\text{cm}^2$)	E_{pit} (mV _{SCE})	i_{pass} ($\mu\text{A}/\text{cm}^2$)
Si-0.0	-249	4.72×10^{-1}	-62.42	15.95
Si-0.1	-270	6.20×10^{-1}	-48.56	5.01
Si-0.2	-317	5.61×10^{-1}	-98.08	3.20
Si-0.3	-383	6.59×10^{-1}	-184.43	17.29
Si-0.4	-454	25.0×10^{-1}	-173.20	98.01

the Nyquist plot when the Si molar ratio ≤ 0.3 , as shown in Fig. 5(a); this indicates that the passivation mechanism of the samples is similar when the Si content is below 0.3. The diameter of the semi-arc first increases and then decreases with an increasing Si content, showing a time constant. The equivalent circuit is shown in Fig. 5(a). When the Si content is 0.4, the Nyquist plot changes, as shown in Fig. 5(c). The diffusion tail forms an angle of 45° with the real axis, which is typical Warburg impedance. In addition, the two-phase peaks in the Bode plot (Fig. 5(d)) show two capacitance time constants, indicating that the corrosion process is influenced by other surface state variables when the AC signal passes through the electrode. This may be a weak area or a surface defect in the passivation film.

Equivalent circuit diagrams for the two types of EIS spectra are presented in the insets of Fig. 5 (a) and (c). The constant-phase element (CPE_{1-T}), and charge-transfer resistance of the original plane (R_f) [27] are shown in Fig. 6. As Si content increases from 0 to 0.2, value of CPE_{1-T}

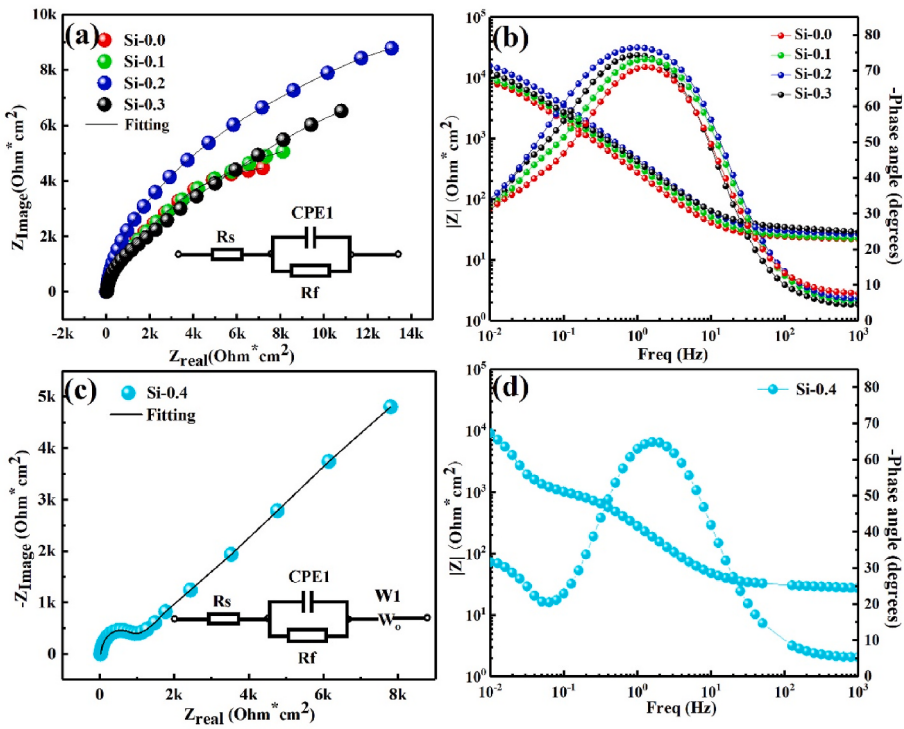


Fig. 5. AC impedance curve of AlCoCrFeNiSi_x HEAs. Nyquist and Bode plots of (a), (b) Si molar ratio ≤ 0.3 HEAs and (c), (d) Si-0.4 HEAs.

reduces from 718.64 to 409.92 μFcm^2 . A suitable Si content improves the protective ability of the passivation film, which can further attack chloride ions. Meanwhile, value of R_f increases from 8957 to 15865 Ωcm^2 . The higher the R_f value, the slower is the corrosion process. However, when Si content is 0.3 and 0.4, CPE_{1-T} value increases to 683.81 μFcm^2 R_f value decreases to 1346 Ωcm^2 . This indicates that a suitable Si content has a positive impact on the formation of a passivation film of AlCoCrFeNi HEAs, whereas excess Si has a negative effect on the formation of a passivation film.

3.3. Morphology after corrosion

The surface morphology of the AlCoCrFeNiSi_x HEAs after electrochemical polarisation testing is shown in Fig. 7. As shown in Fig. 7 (a) and (b), selective corrosion occurred in the DR in the Si-0.0 and Si-0.1 HEAs. Selective corrosion is a type of localised corrosion referred to as localised corrosion (LC). As shown in Fig. 7 (c) and (d), in the Si-0.2 and

Si-0.3 HEAs, localised corrosion is still observed in the DR. In the Si-0.4 HEAs, a large-scale peeling phenomenon occurs on the surface, as indicated by the red line in Fig. 7 (e). This not only implies that the DR is corroded but also that the ID region is dissolved. Corrosion begins by localised corrosion expansion from the first local area and develops into general corrosion.

4. Discussion

4.1. Effect of passivation film on corrosion behaviour

4.1.1. Type of semiconductor

The Mott–Schottky plots of AlCoCrFeNiSi_x HEAs were analysed (Fig. 8). The value of $1/C^2$ in the Si-0.0 HEAs is much smaller than that in the other HEAs and tends towards a straight line. The semiconductor types of the Si-0.0 HEAs are shown in the inset of Fig. 8. Bipolar semiconductor passivation films (P–N heterojunctions) are observed in AlCoCrFeNiSi_x HEAs. The value of $1/C^2$ gradually increases with the addition of Si. In the Si-0.4 HEAs, the value of $1/C^2$ is the highest; this indicates the lowest value of the interfacial capacitance (C). Previous studies have found that the decrease in capacitance can be attributed to an increase in the thickness of the electron-depleted layer and a diminishing number of charge carriers [28]. As the Si content increases, both the inner and outer passivation films are modified, affecting the potential distribution in the electrolyte.

4.1.2. Composition of passivation film

The addition of Si changes the composition of the passivation film, thereby affecting its passivation ability. Therefore, XPS analysis was conducted on the AlCoCrFeNiSi_x HEA. Previous studies have shown that Al and Cr are the main oxides present in Al_xCoCrFeNi HEAs [29] and hybrid steel with Al [30]. Therefore, only Al, Cr, and Si in the AlCoCrFeNiSi_x HEAs were analysed. The fitted Cr, Al and Si peaks are assigned to yellow, red and blue color components, as shown in Fig. 9. When Si molar ratio ≤ 0.2 , the peak area ratio of Cr³⁺/Cr increased with increasing Si content. As the Si content increases, the fitting peaks of Cr

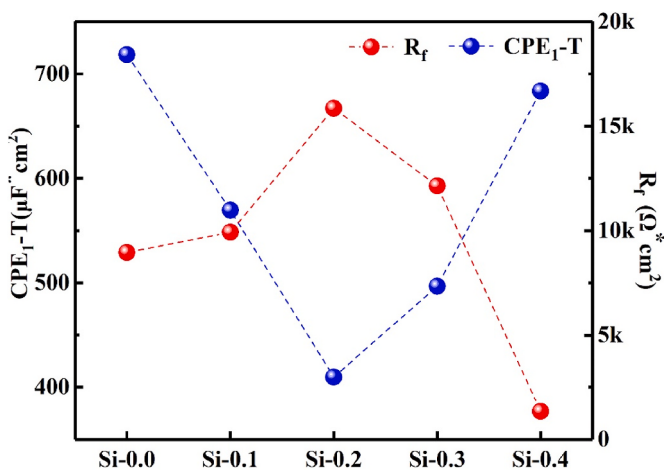


Fig. 6. Values of CPE_{1-T} and R_f of AlCoCrFeNiSi_x HEAs.

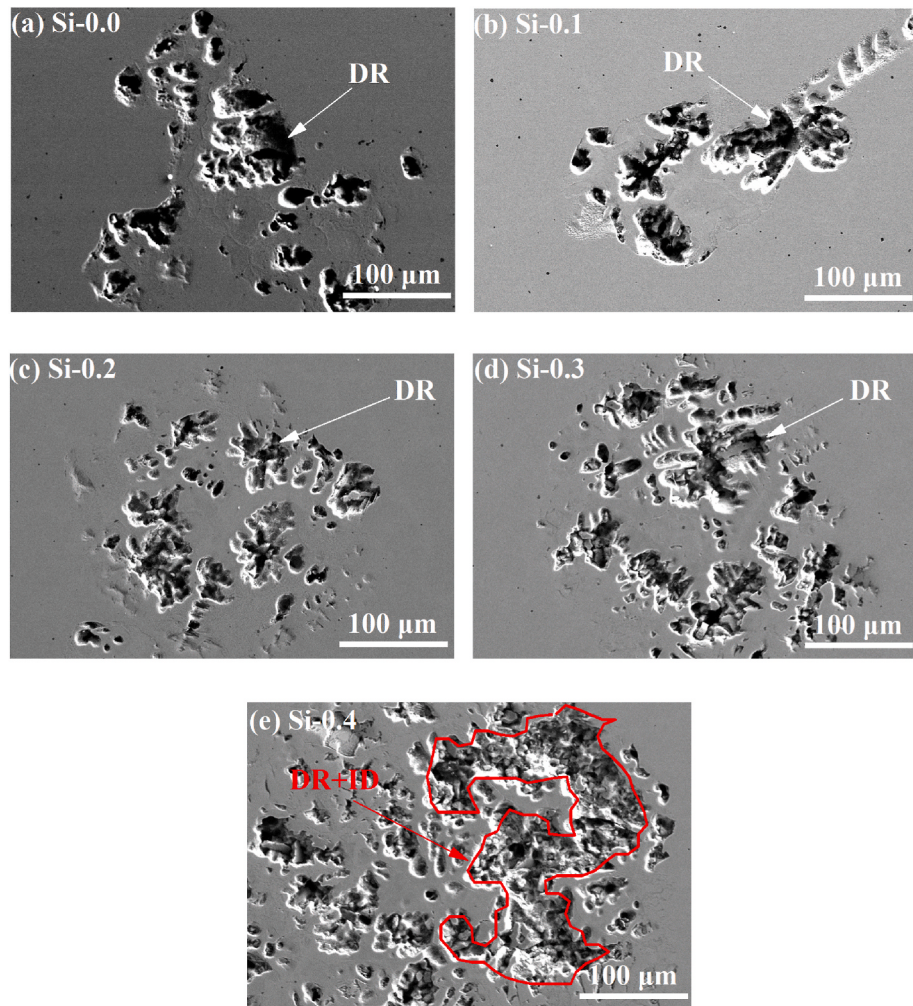


Fig. 7. Corrosion morphology of AlCoCrFeNiSi_x HEAs after potentiodynamic-polarisation testing.

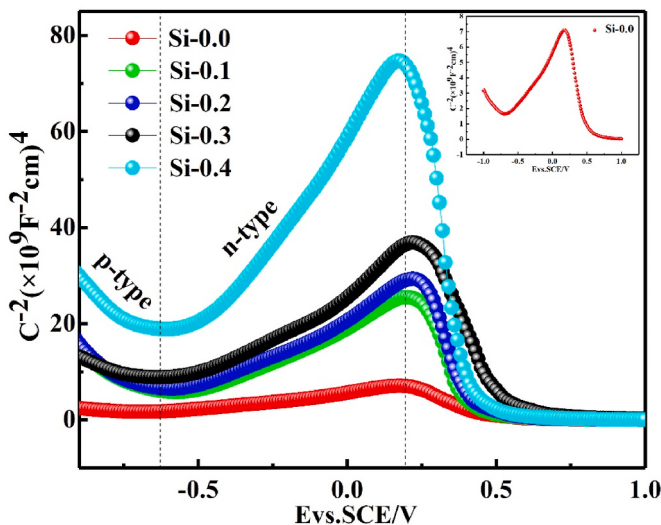


Fig. 8. Mott-Schottky plots of AlCoCrFeNiSi_x HEAs.

becomes unsettled on the passivation films of the Si-0.3 and Si-0.4 HEAs. This indicates that it is beneficial to improve the stability of the Cr passivation films by adding Si. However, excessive Si has an adverse effect of forming a Cr passivation film; this may be attributed to the

formation of silicide doped with Cr, hindering the formation of a Cr passivation film. The peak area ratio of Al³⁺/Al increases with the addition of Si. When Si molar ratio ≥ 0.2 , the passivation film is entirely composed of Al³⁺ and all fitting peaks of Al disappears. These results suggest that Si can improve the stability of the Al passivation film by enhancing its driving force of passivation films. Finally, to further investigate the effect of Si on the passivation film, XPS analysis is performed on Si. A Si passivation film forms on the surface of the AlCoCrFeNi HEAs with Si. The peak ratio of Si²⁺/Si increases with increasing Si.

On the basis of the afore described findings, we conclude that Si enhances the activity of the Al passivation film, resulting in a higher driving force for the passivation film. Suitable addition of Si improves the protectiveness of the Cr passivation film. The Cr passivation film plays a leading role in AlCoCrFeNiSi and AlCoCrFeNi HEAs with a suitable addition of Si exhibiting a stronger passivation ability.

4.2. Effect of crystal structure on corrosion behaviour

4.2.1. Corrosion of spinodal decomposition structure

To investigate the corrosion mechanism of spinodal decomposition, the nano-microscopic observations are conducted on the AlCoCrFeNi HEAs with Si by TEM as shown in Fig. 10. As shown in regions A, B, C, and D in Fig. 10, a periodic nanoscale structure with a size of several hundred nanometres contains alternating bright and dark interconnected phases. The side plate-like microstructure is called spinodal decomposition structure which is composed of ordered B2 phase and disordered A2 phase [31,32]. Si additions could not change B2 into D03

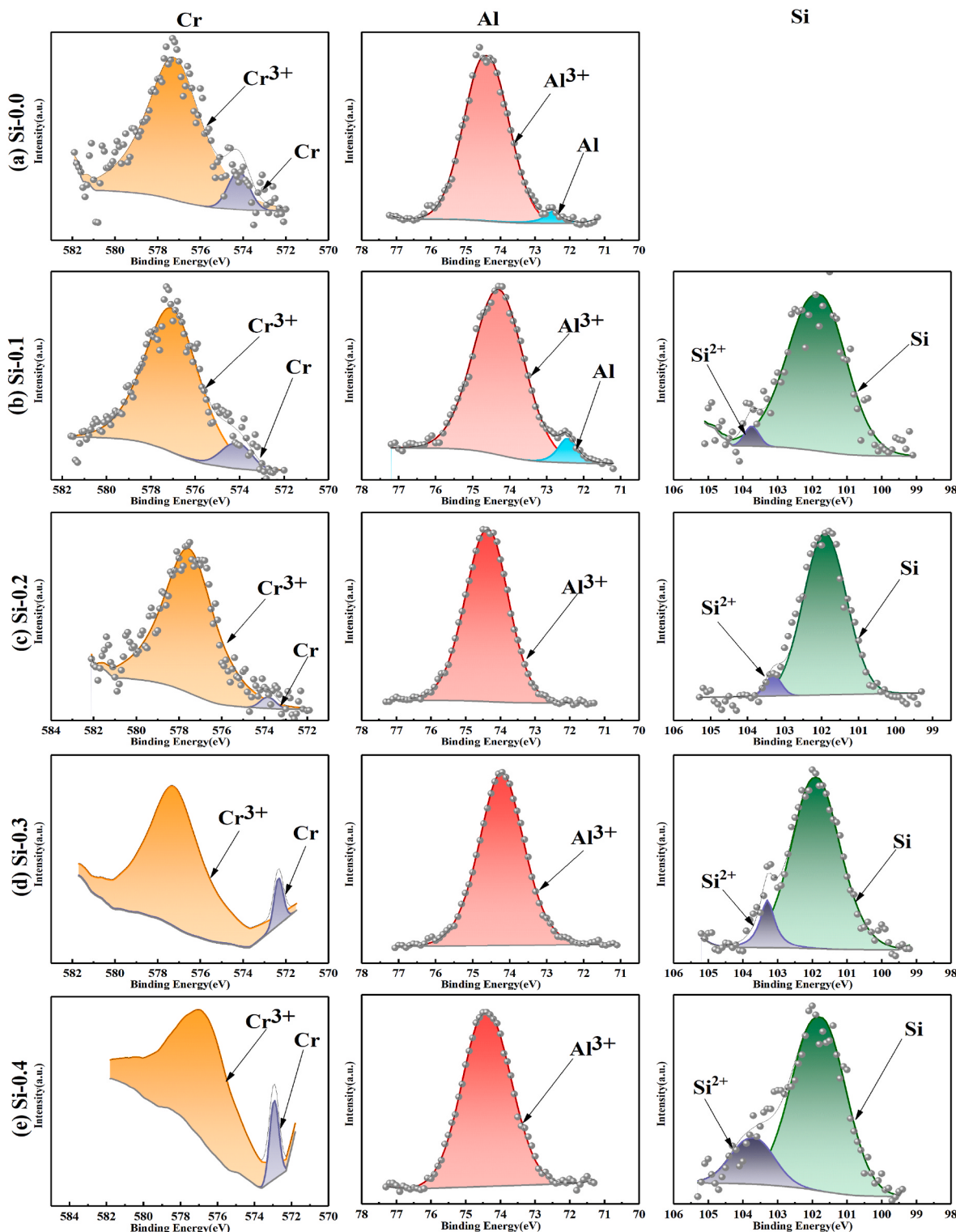


Fig. 9. XPS spectra of Cr₂p_{3/2}, Al₂p_{3/2} and Si₂p_{3/2} of the passivation films formed on AlCoCrFeNiSi_x HEAs.

intermetallic phase, this is also a new research perspective that is different from the novel austenitic lightweight Fe–Mn–Al–Si–C steel [33]. Numerous studies have shown that the A2 phase of AlCoCrFeNi HEAs is composed of an Fe–Cr phase [34]. In the AlCoCrFeNiSi_x HEAs, the diffraction speckle in regions A, B, C, and D suggest that Si is doped into the A2 phase to form the Fe–Cr–Si phase. The size of the A2 phase gradually decreases and the quantity increases with an increasing Si content. The size of the nanoscale precipitates decreases from 400 to

100 nm, and other studies have reported similar results [35]. In our previous study, we found that the B2 phase in the spinodal decomposition structure is attacked by chloride ions. Many small A2 phases are likely to reduce the attack of chloride ions, making it difficult for chloride ions to attack the interior of the B2 phase and cause LC in the spinodal decomposition region. Thus, the Si-0.4 HEAs exhibits better resistance to localised corrosion than the AlCoCrFeNi HEAs with a slight addition of Si.

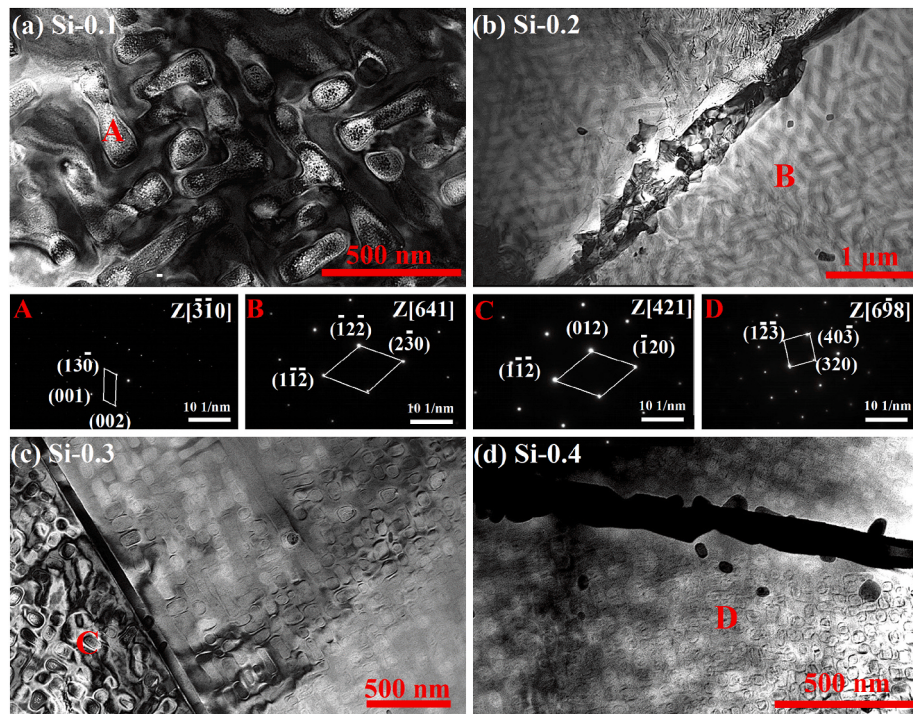


Fig. 10. Nano-microscopic observation of as-cast AlCoCrFeNiSi_x ($x = 0.0, 0.1, 0.2, 0.3$, and 0.4) HEAs via TEM.

4.2.2. Corrosion of dendritic structure

A clearer corrosion morphology was characterised using laser confocal microscopy (LSCM), as shown in Fig. 11. Evident LC occurs on the surfaces of the Si-0.0 and Si-0.1 HEAs, including the petal-like DR and the spinodal decomposition region (B2), as shown in Fig. 11 (a) and (b). When the Si contents are 0.2 and 0.3, localised corrosion still occurs in the DR and spinodal decomposition region (B2), as shown in Fig. 11 (c) and (d). The colour of the spinodal decomposition region becomes lighter, indicating that the degree of corrosion gradually decreases.

When the Si content is 0.4, the colour of the spinodal decomposition region is the lightest, and it is difficult for chloride ions to attack, as shown in Fig. 11 (e). The LSCM images show peeling on the surface of the Si-0.4 HEAs. These results suggest that corrosion occurred in the dendritic and ID regions. At this stage, the corrosion type of the Si-0.4 HEAs changed from local to general corrosion.

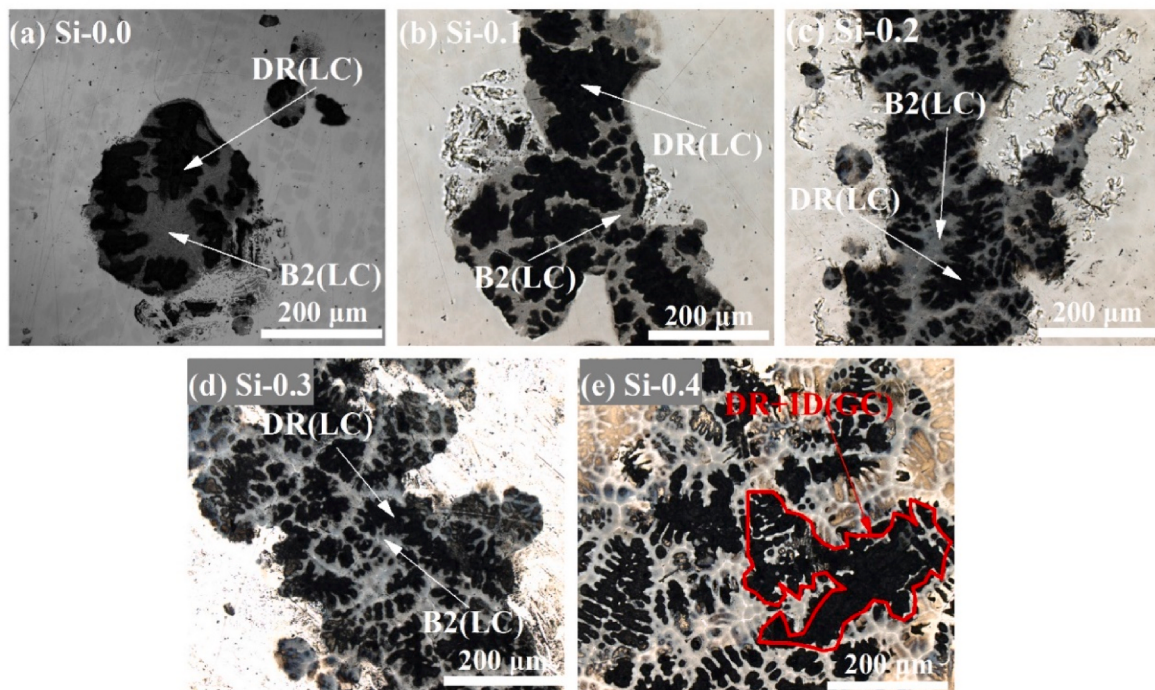


Fig. 11. Corrosion morphology of AlCoCrFeNiSi_x HEAs via laser scanning confocal microscopy.

4.3. Corrosion mechanism

On the basis of the afore described analysis, a corrosion process can be proposed for AlCoCrFeNiSi_x HEAs, as shown schematically in Fig. 12. The colour yellow means DR, the colour green means ID, the colour blue means B2, the colour black means A2, the colour red in ID means silicide, the colour white means corroded, the colour light blue means slightly corroded. The before and after suffered corrosion of Si-0.0 and Si-0.1 HEAs were observed, as shown in Fig. 12 (a) and (b), respectively. The LC was selective corrosion, and the corrosion regions included dendritic (Al–Ni phase) and spinodal decomposition (Al–Ni phase) regions. The corrosion processes of Si-0.2 and Si-0.3 HEAs are shown in Fig. 12 (c) and (d), respectively. In the DR, the area of the ID region (Fe–Cr–Si phase) increased, and the area of the DR (Al–Ni phase) decreased with increasing Si content, as shown in Fig. 12 (c). The size of the A2 phase in the spinodal decomposition region gradually decreased, and the quantity increased. A large amount of small-sized A2 phase decreased the attack of chloride ions on the B2 phase. The dendritic region was mainly corroded by chloride ions. As shown in Fig. 12 (e) and (f), when the Si content was 0.4 in the spinodal decomposition region, the A2 phase was a dense nanoscale precipitate on the B2 matrix, which could effectively prevent the B2 phase from contacting the chloride ions. In the dendritic region, silicide increased with an increasing Si content, which accelerated the corrosion rate in the ID regions (Fe–Cr–Si phase). Both the dendritic and ID regions were corroded. Peeling occurred over a large area on the surface. The type of corrosion changed from localised to general corrosion.

5. Conclusions

Corrosion resistance of the AlCoCrFeNiSi_x HEAs in 3.5 wt% NaCl solution was analysed. The corrosion behaviour of AlCoCrFeNiSi_x was examined from the perspectives of the passivation film and microstructure, and a corrosion mechanism was proposed. The main

conclusions drawn from this study are as follows:

- 1) Si, along with Fe and Cr in AlCoCrFeNi HEAs, segregated into the ID region, which transitioned from a petal shape to a dendritic shape with an increasing Si content.
- 2) The addition of Si promoted phase separation in the spinodal decomposition region. The size of the A2 phase decreased and the amount of the A2 phase increased; this resulted in excellent local corrosion inhibition performance.
- 3) The passive current density of AlCoCrFeNiSi_{0.2} HEAs was 3.2 $\mu\text{A}/\text{cm}^2$, and its corrosion resistance was optimum. This was because the addition of Si improved the protectiveness of the Cr and Al passivation films.
- 4) As a result of a large amount of silicide formed, the corrosion type changed from localised corrosion of AlCoCrFeNiSi_x (molar ratio $x \leq 0.3$) HEAs to general corrosion of AlCoCrFeNiSi_{0.4} HEAs.

Funding

The work was supported by the Open Project of the State Key Laboratory of Light Alloy Casting Technology for High-end Equipment [grant number LACT-009] and Nature Science Foundation of Liaoning Province [grant number 2021-BS-150 and 2022- BS-181].

CRediT authorship contribution statement

Yi Wang: Conceptualization, Formal analysis, Methodology, Software, Writing – original draft. **Guanglong Li:** Conceptualization, Funding acquisition, Resources, Supervision, Writing – review & editing. **Hao Qi:** Investigation, Visualization. **Wei Zhang:** Conceptualization, Funding acquisition, Resources. **Ruirun Chen:** Supervision, Writing – review & editing. **Ruiming Su:** Resources, Supervision. **Bo Yu:** Software, Validation. **Yingdong Qu:** Visualization, Writing – review & editing.

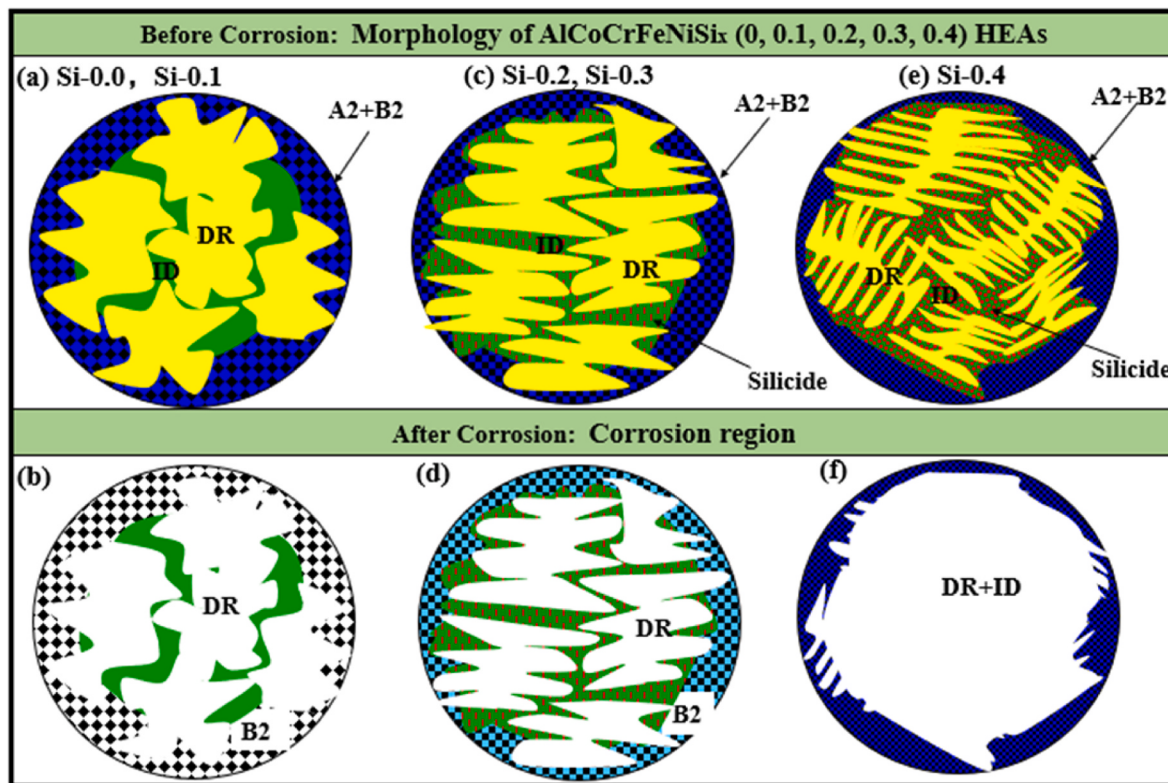


Fig. 12. Schematics of corrosion processes of AlCoCrFeNi HEAs with various Si content. (a), (b) Si-0.0, Si-0.1; (c), (d) Si-0.2, Si-0.3; and (e), (f) Si-0.4.

Declaration of competing interest

The authors declare that they have no known competing financial interests or personal relationships that could have appeared to influence the work reported in this paper.

Data availability

Data will be made available on request.

References

- [1][1] Y.P. Wang, B.S. Li, M.X. Ren, C. Yang, H.Z. Fu, Microstructure and compressive properties of AlCrFeCoNi high entropy alloy, Mater. Sci. Eng. 491 (2008) 154–158, <https://doi.org/10.1016/j.msea.2008.01.064>.
- [2] Z. Tang, M.C. Gao, H.Y. Diao, T.F. Yang, J.P. Liu, T.T. Zuo, Y. Zhang, Z.P. Lu, Y. Q. Cheng, Y.W. Zhang, K.A. Dahmen, P.K. Liaw, T. Egami, Aluminum alloying effects on lattice types, microstructures, and mechanical behavior of high-entropy alloys systems, JOM 65 (2013) 1848–1858, <https://doi.org/10.1007/s11837-013-0776-z>.
- [3] E. Strumza, S. Hayun, Comprehensive study of phase transitions in equiatomic AlCoCrFeNi high-entropy alloy, J. Alloys Compd. 856 (2020) 1873–4669, <https://doi.org/10.1016/j.jallcom.2020.158220>.
- [4] C. Zhao, J. Li, Y. Liu, Y. Wang, C. Kou, E. Beaugnon, J. Wang, Tailoring mechanical and magnetic properties of AlCoCrFeNi high-entropy alloy via phase transformation, J. Mater. Sci. Technol. 73 (2021) 83–90, <https://doi.org/10.1016/j.jmst.2020.08.063>.
- [5] Y. Qiu, S. Thomas, D. Fabijanic, A.J. Barlow, H.L. Fraser, N. Birbilis, Microstructural evolution, electrochemical and corrosion properties of $\text{Al}_x\text{CoCrFeNiTi}_y$ high entropy alloys, Mater. Des. 170 (2019) 107698, <https://doi.org/10.1016/j.matdes.2019.107698>.
- [6] W.R. Wang, W.L. Wang, J.W. Yeh, Phases, microstructure and mechanical properties of $\text{Al}_x\text{CoCrFeNi}$ high-entropy alloys at elevated temperatures, J. Alloys Compd. 589 (2014) 143–152, <https://doi.org/10.1016/j.jallcom.2013.11.084>.
- [7] Y.F. Kao, T.J. Chen, S.K. Chen, J.W. Yeh, Microstructure and mechanical property of as-cast, homogenized and -deformed $\text{Al}_x\text{CoCrFeNi}$ ($0 \leq x \leq 2$) high-entropy alloys, J. Alloys Compd. 488 (2009) 57–64, <https://doi.org/10.1016/j.jallcom.2009.08.090>.
- [8] R. Wang, K. Zhang, C. Davies, X. Wu, Evolution of microstructure, mechanical and corrosion properties of AlCoCrFeNi high-entropy alloy prepared by direct laser fabrication, J. Alloys Compd. 694 (2017) 971–981, <https://doi.org/10.1016/j.jallcom.2016.10.138>.
- [9] Y. Garip, N. Ergin, O. Ozdemir, Resistance sintering of CoCrFeNiAl_x ($x = 0.7, 0.85, 1$) high entropy alloys: Microstructural characterization, oxidation and corrosion properties, J. Alloys Compd. 877 (2021) 160180, <https://doi.org/10.1016/j.jallcom.2021.160180>.
- [10] J. Lu, L. Li, H. Zhang, Y. Chen, P. Xiao, Oxidation behavior of gas-atomized AlCoCrFeNi high-entropy alloy powder at 900–1100°C, Corros. Sci. 181 (2021) 109257, <https://doi.org/10.1016/j.corsci.2021.109257>.
- [11][1] Q. Tian, G. Zhang, K. Yin, W. Wang, W. Cheng, Y. Wang, The strengthening effects of relatively lightweight AlCoCrFeNi high entropy alloy, Mater. Char. 151 (2019) 302–309, <https://doi.org/10.1016/j.matchar.2019.03.006>.
- [11][2] C.P. Lee, C.C. Chang, Y.Y. Chen, J.W. Yeh, H.C. Shih, Effect of the aluminium content of $\text{Al}_x\text{CrFe}1.5\text{MnNi}0.5$ high-entropy alloys on the corrosion behaviour in aqueous environments, Corrosion Sci. 50 (2008) 2053–2060, <https://doi.org/10.1016/j.corsci.2008.04.011>.
- [11][3] Y.Z. Shi, L. Collins, R. Feng, C. Zhang, N. Balk, P.K. Liaw, B. Yang, Homogenization of AlCoCrFeNi high-entropy alloys with improved corrosion resistance, Corrosion Sci. 133 (2018) 120–131, <https://doi.org/10.1016/j.corsci.2018.01.030>.
- [14] S. Shuang, Z.Y. Ding, D. Chung, S.Q. Shi, Y. Yang, Corrosion resistant nanostructured eutectic high entropy alloy, Corrosion Sci. 164 (2019) 108315, <https://doi.org/10.1016/j.corsci.2019.108315>.
- [11][5] C. Dai, T. Zhao, C. Du, Z. Liu, D. Zhang, Effect of molybdenum content on the microstructure and corrosion behavior of FeCoCrNiMo_x high-entropy alloys, J. Mater. Sci. Technol. 46 (2020) 64–73, <https://doi.org/10.1016/j.jmst.2019.10.020>.
- [11][6] C. Xiang, Z.M. Zhang, H.M. Fu, E.H. Han, H.F. Zhang, J.Q. Wang, Microstructure and corrosion behaviour of $\text{AlCoCrFeNiSi}_{0.1}$ high-entropy alloy, Intermetallics 114 (2019) 106599, <https://doi.org/10.1016/j.intermet.2019.106599>.
- [1][7] C. Chen, H. Zhang, Y.Z. Fan, R. Wei, W.W. Zhang, T. Wang, T. Zhang, K. Wu, F. S. Li, S.K. Guan, J.Z. Jiang, Improvement of corrosion resistance and magnetic properties of $\text{FeCoNiAl}_{0.2}\text{Si}_{0.2}$ high entropy alloy via rapid-solidification, Intermetallics 122 (2020) 106778, <https://doi.org/10.1016/j.intermet.2020.106778>.
- [18] Y. Li, P. Zhang, J. Zhang, Z. Chen, B.L. Shen, Oxidation behavior of AlCoCrFeNiSi_x high-entropy alloys at 1100°C, Corrosion Sci. 190 (2021) 109633, <https://doi.org/10.1016/j.corsci.2021.109633>.
- [1][9] B. Gorr, F. Muelle, H.J. Christ, T. Mueller, H. Chen, A. Kauffmann, M. Heilmairer, High temperature oxidation behavior of an equimolar refractory metal-based alloy 20Nb–20Mo–20Cr–20Ti–20Al with and without Si addition, J. Alloys Compd. 688 (2016) 468–477, <https://doi.org/10.1016/j.jallcom.2016.07.219>.
- [20] J.M. Zhu, H.M. Fu, H.F. Zhang, A.M. Wang, H. Li, Z.Q. Hu, Synthesis and properties of multiprincipal component AlCoCrFeNiSi_x alloys, Mater. Sci. Eng. A 527 (2010) 7210–7214, <https://doi.org/10.1016/j.msea.2010.07.049>.
- [21] W.D. Xue, X.M. Yang, X.X. Ye, L. Han, J.Q. Wang, V. Ignatiev, X.T. Zhou, Effects of silicon carbide on the corrosion of metallic materials in molten LiF-NaF-KF salt, Corrosion Sci. 143 (2018) 157–165, <https://doi.org/10.1016/j.corsci.2018.08.023>.
- [22] A. Takeuchi, A. Inoue, Calculations of mixing enthalpy and mismatch entropy for ternary amorphous alloys mater, OR Trans. 1 (2000) 1372–1378, <https://doi.org/10.2320/matertrans1989.41.1372>.
- [23] S.Y. Ma, R.M. Su, G.L. Li, Y.D. Qu, D.R. Li, Effect of deep cryogenic treatment on corrosion resistance of AA7075-RRA, J. Phys. Chem. Solid. 167 (2022) 117470, <https://doi.org/10.1016/j.jpcs.2022.110747>.
- [24] W. Qi, J. Wang, X. Li, Y. Cui, Y. Zhao, J. Xie, G. Zeng, Q. Gao, T. Zhang, F. Wang, Effect of oxide scale on corrosion behavior of HP-13Cr stainless steel during well completion process, J. Mater. Sci. Technol. 64 (2021) 153–164, <https://doi.org/10.1016/j.jmst.2019.10.009>.
- [25] C. Wang, R. Ma, Y. Zhou, Y. Liu, E. Daniel, X. Li, P. Wang, J. Dong, W. Ke, Effects of rare earth modifying inclusions on the pitting corrosion of 13Cr4Ni martensitic stainless steel, J. Mater. Sci. Technol. 93 (2021) 232–243, <https://doi.org/10.1016/j.jmst.2021.03.014>.
- [26] J. Ge, Y. Cui, J. Qian, L. Liu, F. Meng, F. Wang, Morphology-controlled CoNi/C hybrids with bifunctions of efficient anti-corrosion and microwave absorption, J. Mater. Sci. Technol. 102 (2022) 24–35, <https://doi.org/10.1016/j.jmst.2021.07.003>.
- [27] Z.H. Jin, H.H. Ge, W.W. Lin, Y.W. Zong, S.J. Liu, J.M. Shi, Corrosion behaviour of 316L stainless steel and anti-corrosion materials in a high acidified chloride solution, Appl. Surf. Sci. 322 (2014) 47–56, <https://doi.org/10.1016/j.apsusc.2014.09.205>.
- [28] S. Ningshen, U.K. Mudali, V.K. Mittal, H.S. Khatak, Semiconducting and passive film properties of nitrogen-containing type 316LN stainless steels, Corrosion Sci. 49 (2007) 481–496, <https://doi.org/10.1016/j.corsci.2006.05.041>.
- [29] Y.Z. Shi, B. Yang, X. Xie, J. Brecht, K.A. Dahmen, P.K. Liaw, Corrosion of $\text{Al}_x\text{CoCrFeNi}$ high-entropy alloys: Al-content and potential scan-rate dependent pitting behavior, Corrosion Sci. 119 (2017) 33–45, <https://doi.org/10.1016/j.corsci.2017.02.019>.
- [30] C. Örnek, B. Payam, A. Gloskovskii, K. Kazmanli, N. Mohamed, B. Derin, M. Ürgen, C.E. Chou, H.W. Yen, B. Avci, S. Ooi, Understanding the passive behaviour of low-chromium high-strengthHybridsteel in corrosive environments, Npj. 7 (2023) 71, <https://doi.org/10.1038/s41529-023-00392-z>.
- [31] W.W. Yu, Y.D. Qu, C.Z. Li, Z. Li, Y.F. Zhang, Y.Z. Guo, J.H. You, R.M. Su, Phase selection and mechanical properties of $(\text{Al}21.7\text{Cr}15.8\text{Fe}28.6\text{Ni}33.9)(\text{x})$ ($\text{Al}9.4\text{Cr}19.7\text{Fe}41.4\text{Ni}29.5)(100-\text{x})$ high entropy alloys, Mater. Sci. & Eng. A. 751 (2019) 754–759, <https://doi.org/10.1016/j.msea.2019.02.067>.
- [32] W.R. Wang, W.L. Wang, S.C. Wang, Y.C. Tsai, C.H. Lai, J.W. Yeh, Effects of Al addition on the microstructure and mechanical property of $\text{Al}_x\text{CoCrFeNi}$ high-entropy alloys, Intermetallics 26 (2012) 44–51, <https://doi.org/10.1016/j.intermet.2012.03.005>.
- [33] Z.H. Lai, Y.H. Sun, Y.T. Lin, J.F. Tu, H.W. Yen, Mechanism of twinning induced plasticity in austenitic lightweight steel driven by compositional complexity, Acta Mater. 210 (2021) 116814, <https://doi.org/10.1016/j.actamat.2021.116814>.
- [34] J. Lu, Y. Chen, H. Zhang, L. Li, L.M. Fu, X.F. Zhao, F.W. Guo, P. Xiao, Effect of Al content on the oxidation behavior of Y/Hf-doped AlCoCrFeNi high-entropy alloy, Corrosion Sci. 170 (2020) 108691, <https://doi.org/10.1016/j.corsci.2020.108691>.
- [35] L. Wojciech, S. Monika, K.G. Mariola, G. Piotr, R. Adrian, W. Tymon, Z. Katarzyna, B. Rafal, The effect of cooling rate on the structure and selected properties of AlCoCrFeNiSi_x ($x = 0; 0.25; 0.5; 0.75$) high entropy alloys, J. Alloys Compd. 905 (2022) 164074, <https://doi.org/10.1016/j.jallcom.2022.164074>.